INORGANIC CHEMISTRY FRONTIERS

RESEARCH ARTICLE

View Article Online
View Journal | View Issue

Cite this: *Inorg. Chem. Front.*, 2024, **11**, 1775

From $(NH_4)_3[Zr(PO_4)_2F]$ to $(NH_4)_3[Sn_2(PO_4)_2]Cl$: the rational design of a tin-based short-wave ultraviolet phosphate with large optical anisotropy†

Zhi Fang,[a,c] Wen-Hua Ma,[b] Qiu-Yu Chen,[b] Xin-Ting Zhu,[a] Xin-Mei Zeng,[a] Pei-Bei Li,[a] Qian-Fen Zhou,[a] Ting-Ting Song[b] and Mei-Hong Duan *[b]

Received 12th December 2023,
Accepted 30th January 2024

DOI: 10.1039/d3qi02561f

rsc.li/frontiers-inorganic

Exploration of ultraviolet phosphates with large optical anisotropy is of great significance to the development of ultraviolet lasers. Nevertheless, featuring a highly-symmetric structural unit of the PO_4 group, ultraviolet phosphates are usually characterized by small optical anisotropies in spite of the discovery of numerous phosphates, highlighting the great challenge in the design and synthesis of benign ultraviolet phosphates. Herein, a new ultraviolet phosphate of $(NH_4)_3[Sn_2(PO_4)_2]Cl$ was rationally obtained by a substitution-oriented design strategy. With the cosubstitution of Zr^{4+} and out-of-plane F^- of $[Zr(PO_4)_2F]_\infty^{3-}$ layers of $(NH_4)_3[Zr(PO_4)_2F]$, $(NH_4)_3[Sn_2(PO_4)_2]Cl$ featuring new layers of $[Sn_2(PO_4)_2]_\infty^{2-}$ and out-of-plane Cl^- was successfully isolated, indicating the feasibility of substitution for the design of $(NH_4)_3[Zr(PO_4)_2F]$-type phosphates. In particular, $(NH_4)_3[Sn_2(PO_4)_2]Cl$ exhibits a wide band gap of 4.7 eV and a large birefringence of 0.065 @ 1064 nm, which is favorable to practical applications.

Introduction

Benefiting from their prominent physicochemical properties and diverse structures, non-π-conjugated phosphates and sulphates have been stellar materials in ion exchange,[1,2] catalysis,[3,4] nonlinear optics,[5–7] *etc*. In particular, with the intrinsic solar-blind nature of P–X (where X = O, F and Cl) bonds and their comprehensive advantages over physicochemical stabilities, phosphates are desirable ultraviolet crystals with exceptional performance for optical transparency and laser damage threshold, which has enabled the extensive application of $KTiPO_5$ [8–10] and KH_2PO_4 (KDP)[11–13] crystals in the near ultraviolet and visible light region. In contast, in terms of the valuable short-wave ultraviolet (SUV, $\lambda < 280$ nm) region, there are still few mature nonlinear optical (NLO) phosphates, which can be ascribed to the tremendous difficulty of the coexistence of a moderate optical dispersion ability ($\Delta n \geq 0.04$ @ 1064 nm) and a wide band gap ($E_g \geq 4.4$ eV) in one specific phosphate. For instance, the remarkable crystal of $LiHgPO_4$ [14] was characterized by a large birefringence of 0.068 @ 1064 nm together with a small band gap of 4.03 eV, while the notably deep-UV ($\lambda < 200$ nm) transparent crystal of $Ba_5P_6O_{20}$ [15] was predicted to have a weak optical dispersion ability. Hence, the exploration of ultraviolet phosphates with large optical anisotropy is of great significance.

Hitherto, several strategies have been applied to the enhancement of optical dispersion abilities of phosphates. Generally, they can be classified into two categories, namely the introduction of birefringence-active (BA) units like anionic groups with large structural anisotropies aroused by stereoactive lone pair (SALP) electrons or π-conjugated configurations, as well as the utilization of low dimensional anionic frames like one-dimensional chains and two-dimensional layers. According to Pauling's 4th rule, most π-conjugated anionic groups and phosphate groups should be inherently repulsive to each other for their small coordination numbers and high valence central cations, detrimental to the molecular design. In contrast, despite their outstanding performance over optical anisotropy and competitive structural affinity to phosphate groups, SALP-type anionic groups are usually excluded from SUV phosphates for their fatal impact on optical transparence. Surprisingly, recent investigations of SALP-type materials have revealed that antimony- and tin-based SALP-type anionic groups are supportive of the coexistence of a large birefringence and wide band gap,[16–19] while the rarity of antimony- and tin-based phosphates, let alone

[a]*Chemical Synthesis and Pollution Control Key Laboratory of Sichuan Province, College of Chemistry and Chemical Engineering, China West Normal University, Nanchong 637002, China*
[b]*College of Physics and Astronomy, China West Normal University, Nanchong 637002, China. E-mail: duanmeihong@126.com*
[c]*State Key Laboratory of Structural Chemistry, Fujian Institute of Research on the Structure of Matter, Chinese Academy of Sciences, Fuzhou, Fujian 350002, P. R. China*

†Electronic supplementary information (ESI) available: Supplementary tables of selected structural information (PDF). CCDC 2313671. For ESI and crystallographic data in CIF or other electronic format see DOI: https://doi.org/10.1039/d3qi02561f

those with one dimensional chains and two dimensional layers, has made the feasibility of antimony- and tin-based SUV phosphates much yet indistinct.

Moreover, to date, the most efficient way to design inorganic crystals with specific structures is through substitution using appropriate prototypes and substitutes, with the selection of the prototype playing a vital role in determining the outcome. By searching the Inorganic Crystal Structure Database, the famous zirconium phosphate $(NH_4)_3[Zr(PO_4)_2F]$[20] (abbreviated as AZPOF) has caught our attention due to its merits. These include two-dimensional layers of $[Zr(PO_4)_2F]^{3-}_{\infty}$ with advantages in terms of structural anisotropy, weak interlayer hydrogen bonding resulting in high structural flexibility to accommodate layer variations, and the utilization of highly electronegative F^- ions to expand the band gap. Most importantly, Zr^{4+} was proved to be substitutable by Sb^{3+} and Sn^{2+}, which has enabled the achievement of a series of $NaTi_2(PO_4)_3$-type[21] antimony- and tin-based phosphates. Hence, AZPOF-type antimony- and tin-based phosphates should have high feasibility for synthesis, as well as high capacity for optical anisotropy and SUV transparency.

Prompted by these actualities, we focused on the exploration of AZPOF-type antimony- and tin-based phosphates through substitution. Fortunately, $(NH_4)_3[Sn_2(PO_4)_2]Cl$ (abbreviated as ASPOC), the first AZPOF-type tin-based phosphate, was obtained. ASPOC not only features AZPOF-type $[Sn_2(PO_4)_2]^{2-}_{\infty}$ layers, but also exhibits SUV transparency and a large birefringence of 0.065 @ 1064 nm. Herein, we introduce the synthesis, structure and properties of ASPOC.

Experimental

Synthesis and crystal growth

Single crystals of ASPOC were grown using a mild hydrothermal method. The growth was carried out by mixing $C_3N_3(NH_2)_3$, $(NH_4)H_2PO_4$ and $SnCl_2{\cdot}2H_2O$ in a molar ratio of approximately (2–4) : (4–6) : (1–2), along with HCl acid (**Caution**: the addition of HCl should be done in a fume cupboard due to its volatility and corrosiveness) and H_2O solvent. The corresponding ingredients were then poured into 25 mL Teflon-lined autoclaves, which were securely sealed in high-pressure reaction vessels. The autoclaves were heated slowly to 170 °C in an oven and maintained at this temperature for approximately three days. Afterward, the mixtures were slowly cooled to room temperature within one day, leading to the precipitation of ASPOC. Block-shaped crystals were selected for single crystal X-ray diffraction (XRD) measurement, while polycrystalline samples were also chosen for property characterization. The purity of polycrystalline samples of ASPOC was evaluated using powder XRD measurement (Fig. S1†).

X-ray diffraction measurements

An ASPOC crystal measuring 0.12 × 0.12 × 0.07 mm^3 was selected for single crystal X-ray diffraction data collection. The data were collected using an Agilent Technologies Super Nova Dual Wavelength CCD diffractometer equipped with graphite-monochromatic Mo Kα radiation (λ = 0.71073 Å) at 297.34(11) K. The crystal structure was solved using the intrinsic phasing method with ShelXT[22] and refined using full matrix least squares techniques with ShelXL.[23] Based on the unusual temperature factors observed for fully-occupied 'Cl1', the presence of a prominent residual peak near 'Cl1', and the significantly large R_1 index, it is highly probable that the splitting of 'Cl1' was required. To substantiate this hypothesis, the split position of 'Cl2' was primarily determined based on the aforementioned residual peak, and the occupancy was obtained through a free refinement using ShelXL. The considerably decreased R_1 index and the well-normalized temperature factors of both 'Cl1' and 'Cl2' further validated the correctness of this arrangement. The accuracy of the structure was verified using the ADDSYM algorithm in the PLATON[24] program. PXRD patterns of ASPOC polycrystalline samples were collected by a TongDa TD-3500 diffractometer using Cu Kα radiation (α = 1.5406 Å) at room temperature with an angular range of 2θ = 10–70°, a scan step width of 0.02° and a scan rate of 1.6° min^{-1}.

Optical measurements

The reflection spectrum of ASPOC was performed with a UV 2600 UV-vis spectrophotometer in the range of 200–800 nm, while the reflectance of $BaSO_4$ plate was used as the referential standard.

Thermal analysis

Differential thermal analysis (DTA) was carried out on a NETZSCH STA 2500 analyzer under flowing nitrogen gas. The sample was enclosed in an Al_2O_3 crucible and heated from room temperature to 500 °C at a rate of 15 K min^{-1}.

Computational details

The electronic and optical properties of ASPOC were investigated using density functional theory (DFT) with a plane-wave pseudopotential method. The Perdew–Burke–Ernzerhof (PBE) functional in the generalized gradient approximation (GGA) was chosen as the exchange–correlation functional. A cutoff energy of 750 eV was employed to determine the number of plane-wave basis sets. Monkhorst–Pack k-point sampling was 2 × 3 × 3 for numerical integration over the Brillouin zone. In the optical property calculations, more than 400 empty bands were considered, and a scissors operator value of 0.754 eV was incorporated into the analysis of the refractive indices. A similar setup was used for the theoretical calculation of AZPOF, with some variations. The cutoff energy was increased to 850 eV, and the Monkhorst–Pack k-point sampling was adjusted to 2 × 4 × 3.

Results and discussion

Crystal structures

As listed in Table 1, ASPOC crystalizes in the orthorhombic *Pbcn* space group. The asymmetric unit of ASPOC is consti-

Table 1 Crystallographic data and structure refinement for ASPOC

Empirical formula	$(NH_4)_3[Sn_2(PO_4)_2]Cl$
Space group	*Pbcn*
a/Å	9.6614(15)
b/Å	9.9609(16)
c/Å	13.465(3)
Z	4
μ/mm^{-1}	4.335
F(000)	976.0
Radiation	Mo Kα
2Θ range for data collection/°	5.874 to 59.414
Index ranges	$-13 \le h \le 9$, $-13 \le k \le 13$, $-10 \le l \le 17$
Reflections collected	4098
Independent reflections	1590 [R_{int} = 0.0434, R_{sigma} = 0.0558]
Data/restraints/parameters	1590/0/85
Goodness-of-fit on F^2	1.083
Final *R* indices [$I \ge 2\sigma(I)$]	R_1 = 0.0376, wR_2 = 0.0932
Final *R* indices [all data]	R_1 = 0.0628, wR_2 = 0.1074
Largest diff. peak/hole/e Å^{-3}	0.96/−0.91

$R_1 = \sum||F_o| - |F_c||/\sum|F_o|$, $wR_2 = \{\sum w[(F_o)^2 - (F_c)^2]^2/\sum w[(F_o)^2]^2\}^{1/2}$.

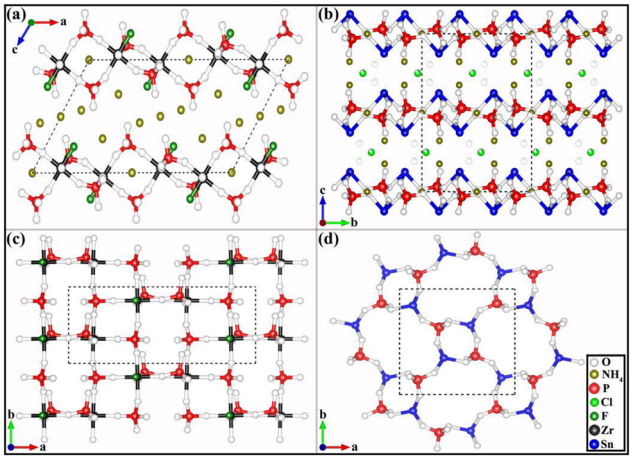

Fig. 1 Comprehensive structural characteristics of AZPOF (a) and ASPOC (b) as well as the layer characteristics of AZPOF (c) and ASPOC (d). (Two disordered partial Cl^- anions with total occupancy of 0.198 are depicted with translucency for better clarity in (b).)

tuted by two chlorine atoms, two nitrogen atoms, one tin atom, one phosphorus atom, four oxygen atoms and eight hydrogen atoms. To be specific, tin cations are all three-coordinated to oxygen atoms of 'O1', 'O2' and 'O3' with bond lengths ranging from 2.093(5) Å to 2.121(5) Å, while phosphorus atoms are all coordinated to four crystallographically-independent oxygen atoms with bond lengths in the range of 1.497–1.539 Å. Such structural parameters for PO_4 and SnO_3 units are close to those in crystals like $Sn_2P_2O_7$ [25] and A$[Sn_4(PO_4)_3]$ (A = Na, K, NH_4).[26] Subsequently, each pair of PO_4 and SnO_3 units formed eight-membered $Sn_2O_2(PO_4)_2$ loops through the alternating sharing of 'O1' and 'O3' atoms between the adjacent PO_4 and SnO_3 units, while each $Sn_2O_2(PO_4)_2$ loop was corner-shared with four $Sn_2O_2(PO_4)_2$ loops through 'O2' atoms in fabricating the open frame work of $[Sn_2(PO_4)_2]_\infty^{2-}$ layers. Consequently, a new type of sixteen-membered $Sn_4O_4(PO_4)_4$ loop with an open area of 5.628 Å × 8.321 Å was generated, while the center of the $Sn_4O_4(PO_4)_4$ loop was occupied by one NH_4 ion, with a central anion of 'N1'. With respect to the inter-layer region of ASPOC, NH_4 ions with a central anion of 'N2' and chlorine ions of 'Cl1' and 'Cl2' are dispersed as counter ions.

As illustrated in Fig. 1, AZPOF and ASPOC have many similarities in terms of structure. To be specific, both of them are characterized by layered structures with inter-layer connections consisting of weak ionic bonds and hydrogen bonds, while the layers in both crystals share similar topologic patterns, including eight-membered and sixteen-membered loops. Hence, ASPOC can be classified as an AZPOF-type crystal. To the best of our knowledge, this is the first time that a new AZPOF-type crystal has been achieved with the uneven substitution of Zr^{4+} with SALP-type Sn^{2+}, highlighting the feasibility of uneven substitution strategy in the exploration of AZPOF-type crystals. On the other hand, the structure of ASPOC reveals certain differences as compared with that of AZPOF due to the uneven substitution. Firstly, with the uneven substitution of Zr^{4+} with SALP-type Sn^{2+}, ASPOC exhibits only corner-sharing between adjacent eight-membered loops, in contrast to the presence of both edge- and corner-sharing between adjacent eight-membered loops in AZPOF. Secondly, ASPOC is characterized by a quasi-coplanar arrangement of PO_4 units and an ambilateral alignment of Sn^{2+} with reference to their anionic layer planes. This contrasts with the ambilateral arrangement of PO_4 units and quasi-coplanar alignment of Zr^{4+} in AZPOF. Last but not least, in contradistinction to the involvement of halogen elements, specifically F^-, in the formation of $[Zr(PO_4)_2F]_\infty^{3-}$ anionic layers in AZPOF, ASPOC excludes halogen elements from the anionic layers of $[Sn_2(PO_4)_2]_\infty^{2-}$.

Thermal analysis

As illustrated in Fig. 2, the DTA curve reveals a palpable endothermic peak at 208.9 °C in the heating process, implying the thermal decomposition of ASPOC. Impressively, no other peaks were detected throughout the entire measurement, suggesting the stability of ASPOC over a wide temperature range. This finding highlights that ASPOC exhibits a higher decomposition temperature compared to other ammonium-included phosphates such as $NH_4[BPO_4F]$,[27] $(NH_4)_3Fe(PO_3F)_2F_2$ [28,29] and $NH_4Fe_2(PO_4)_2$.[30] Hence, the moderate decomposition temperature of ASPOC should contribute to the practical applications of ASPOC.

Optical properties

By referring to the UV-vis diffuse reflection spectrum shown in Fig. 3, ASPOC exhibited remarkable optical transparency within the wavelength range of 350–800 nm by presenting comparable reflection rates to those of the referential $BaSO_4$ powder. To determine the actual band gap of ASPOC, the Kubelka–Munk plot was employed, as demonstrated in the inner chart of Fig. 3. By analyzing the simulated plot in Fig. 3, the band gap of ASPOC was estimated to be approximately 4.7

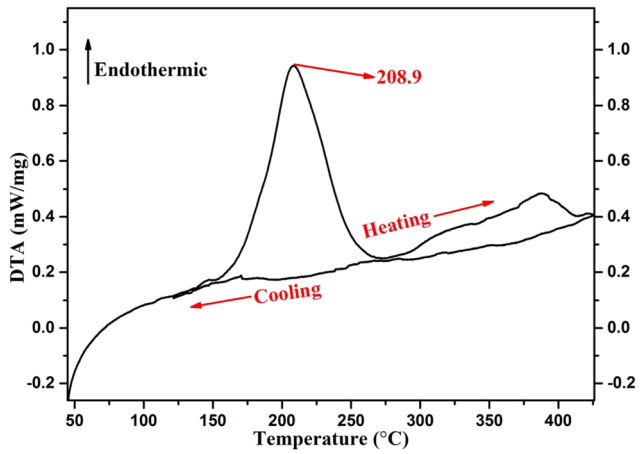

Fig. 2 Measured DTA curve of ASPOC.

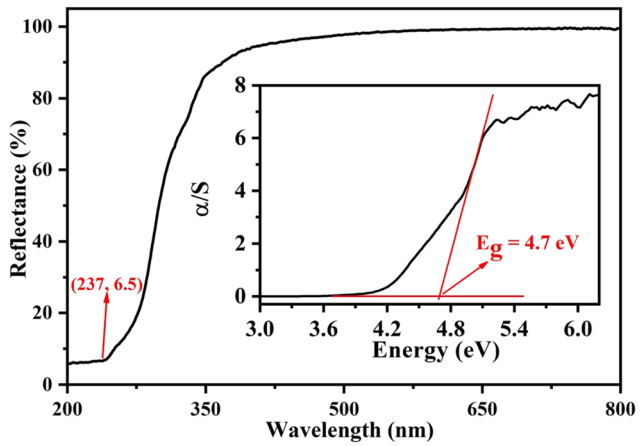

Fig. 3 UV-vis diffuse reflection spectrum (outer chart) and the fitted Kubelka–Munk plot (inner chart) of ASPOC.

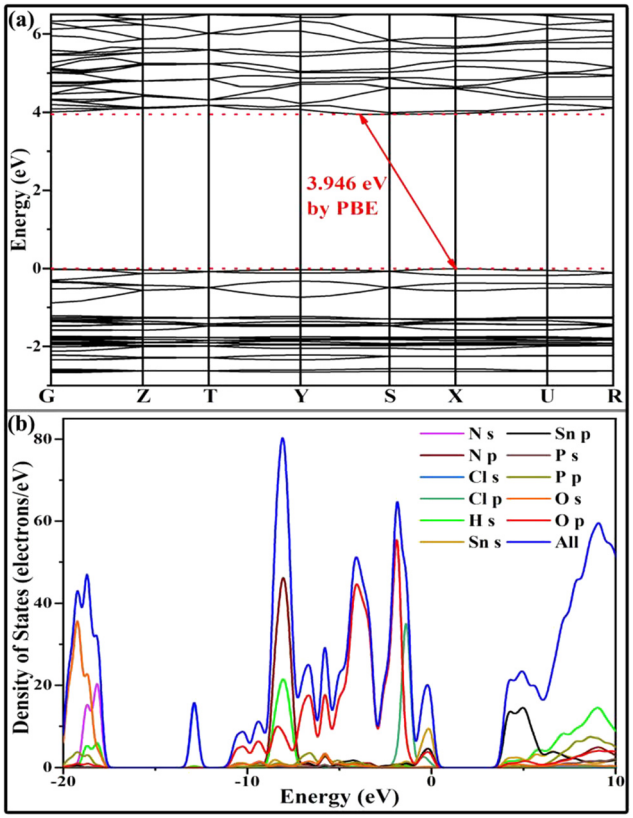

Fig. 4 Calculated band structure (a) and density of states map (b) of ASPOC.

eV. This value aligns well with the colorless appearance of the as-grown crystals of ASPOC, further confirming its high transparency across the visible region. On the other hand, despite experiencing a sharp decrease in light transmission in the UV region, ASPOC still exhibits a distinct short cut-off edge at around 237 nm. The wide transparency window exhibited by ASPOC surpasses those of most stannites, such as $Sn_2Mn(PO_4)_2$,[31] $(NH_4)_4Ag_{12}Sn_7Se_{22}$[32] and $PbSn(PO_4)Cl$,[33] and is comparable to the transparency ranges observed in $Na_3CaZn_2B_3O_9$,[34] $Ba_2(BO_3)_{1-x}(CO_3)_xCl_{1+x}$[35] and $BaZnBO_3F$[36] materials. This characteristic is particularly advantageous for ASPOC in SUV applications, where materials with a broad transparency window are sought after.

Theoretical calculations

To understand the origin of the optical transparency of ASPOC, theoretical calculations were performed using a plane-wave pseudopotential DFT method to analyze its band structure and density of states (DOS) map. As depicted in Fig. 4(a), ASPOC was predicted to be an indirect band gap crystal, with a calculated value of approximately 3.946 eV, slightly underestimated compared to the experimental value obtained. This deviation may be attributed to the discontinuity of the generalized gradient approximation/Perdew–Burke–Ernzerhof (PBE) exchange–correlation potentials.[37] In addition, as shown in Fig. 4(b), the occupied states at the top of the valence band primarily originate from Sn 5s orbitals, accompanied by a minority density of states contributed by Sn 5p, O 2p, and Cl 3p orbitals. Conversely, the states at the bottom of the conduction band are predominantly derived from Sn 5p orbitals. Hence, the band gap of ASPOC is mainly determined by the inherent restrictions imposed by Sn 5s and 5p orbitals, as well as the influence of Sn–O and Sn–Cl bonds.

As an AZPOF-type crystal, the optical dispersion properties of ASPOC are of great interest to us, as they play a crucial role in determining the practical application potential of SUV crystals. In this study, we calculated the refractive index and birefringence of ASPOC, as depicted in Fig. 5. To compensate for the underestimated band gap resulting from the PBE method, a scissors operator of 0.754 eV was introduced. From the calculations, we determined the birefringence of ASPOC to be approximately 0.065 at 1064 nm. For comparison, the birefringence of AZPOF was calculated to be around 0.029 at the same wavelength. Remarkably, the birefringence of ASPOC is found

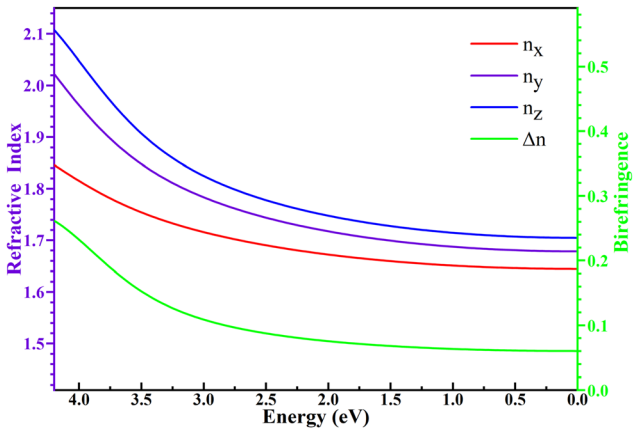

Fig. 5 Calculated refractive index and birefringence of ASPOC.

to be higher than that of practical UV borate crystals such as LiB_3O_5 (0.04 at 1064 nm),[38,39] $NaSr_3Be_3(BO_3)_3F_4$ [40,41] and $BaAl_2B_2O_7$ (0.05 at 1064 nm).[42] This observation suggests that ASPOC holds promising potential for practical applications in the field of UV optics.

Conclusions

In summary, a new ultraviolet phosphate compound, $(NH_4)_3[Sn_2(PO_4)_2]Cl$, was successfully obtained using a substitution-oriented design strategy. This involved the cosubstitution of Zr^{4+} and out-of-plane F^- in the $[Zr(PO_4)_2F]_\infty^{3-}$ layers of $(NH_4)_3[Zr(PO_4)_2F]$ with two Sn^{2+} and Cl^-, resulting in the formation of $(NH_4)_3[Sn_2(PO_4)_2]Cl$ with new layers of $[Sn_2(PO_4)_2]_\infty^{2-}$ and out-of-plane Cl^-. This achievement highlights the possibility of substitution as a viable approach to $(NH_4)_3[Zr(PO_4)_2F]$-type phosphates. In particular, $(NH_4)_3[Sn_2(PO_4)_2]Cl$ exhibits a wide band gap of 4.7 eV and a large birefringence of 0.065 @ 1064 nm, being favorable to practical applications. Given the rarity of $(NH_4)_3[Zr(PO_4)_2F]$-type crystals and the availability of abundant alternative substitutes such as Sb^{3+}, Bi^{3+}, and Pb^{2+} ions, as well as Br^-, $(IO_3)^-$ and I^- anions, there is great potential for the development of $(NH_4)_3[Zr(PO_4)_2F]$-type crystals with advanced properties. Current research endeavors are dedicated to exploring these possibilities.

Conflicts of interest

There are no conflicts of interest to declare.

Acknowledgements

This work was supported by the Sichuan Science and Technology Program (no. 2023NSFSC0957), the Natural Science Foundation of Sichuan Province (no. 2022NSFSC1854, and 2022NSFSC1841), the PhD Research Startup Foundation of China West Normal University (no. 20E070 and 22kE011) and the Key Laboratory of Functional Crystals and Laser Technology, TIPC, CAS (no. FCLT202204).

Notes and references

1 N. I. Chubar, V. A. Kanibolotskyy, V. V. Strelko, G. G. Gallios, V. F. Samanidou, T. O. Shaposhnikova, V. G. Milgrandt and I. Z. Zhuravlev, Adsorption of phosphate ions on novel inorganic ion exchangers, *Colloids Surf., A*, 2005, **255**, 55–63.
2 I. W. Almanassra, G. Mckay, V. Kochkodan, M. A. Atieh and T. Al-Ansari, A state of the art review on phosphate removal from water by biochars, *Chem. Eng. J.*, 2021, **409**, 128211.
3 A. Lee and K. A. Scheidt, A cooperative N-heterocyclic carbene/chiral phosphate catalysis system for allenolate annulations, *Angew. Chem.*, 2014, **126**, 7724–7728.
4 R. S. J. Proctor, A. C. Colgan and R. J. Phipps, Exploiting attractive non-covalent interactions for the enantioselective catalysis of reactions involving radical intermediates, *Nat. Chem.*, 2020, **12**, 990–1004.
5 Y. Li, C. Yin, X. Yang, X. Kuang, J. Chen, L. He, Q. Ding, S. Zhao, M. Hong and J. Luo, A nonlinear optical switchable sulfate of ultrawide bandgap, *CCS Chem.*, 2021, **3**, 2298–2306.
6 Y.-Q. Li, J.-H. Luo, X.-H. Ji and S.-G. Zhao, A short-wave UV nonlinear optical sulfate of high thermal stability, *Chin. J. Struct. Chem.*, 2020, **39**, 485–492.
7 Y. Liu, Y. Liu, Z. Lin, Y. Li, Q. Ding, X. Chen, L. Li, S. Zhao, M. Hong and J. Luo, Nonpolar $Na_{10}Cd(NO_3)_4(SO_3S)_4$ exhibits a large second-harmonic generation, *CCS Chem.*, 2022, **4**, 526–531.
8 D. R. Allan, J. S. Loveday, R. J. Nelmes and P. A. Thomas, A high-pressure structural study of potassium titanyl phosphate (KTP) up to 5 GPa, *J. Phys.: Condens. Matter*, 1992, **4**, 2747.
9 F. Yang, L. Wang, L. Huang and G. Zou, The study of structure evolvement of $KTiOPO_4$ family and their nonlinear optical properties, *Coord. Chem. Rev.*, 2020, **423**, 213491.
10 X. Meng, Z. Wang, W. Tian, J. Song, X. Wang, J. Zhu and Z. Wei, High average power 200 fs mid-infrared KTP optical parametric oscillator tunable from 2.61 to 3.84 μm, *Appl. Phys. B: Lasers Opt.*, 2021, **127**, 129.
11 T. Sasaki and A. Yokotani, Growth of large KDP crystals for laser fusion experiments, *J. Cryst. Growth*, 1990, **99**, 820–826.
12 A. Shaykin, V. Ginzburg, I. Yakovlev, A. Kochetkov, A. Kuzmin, S. Mironov, I. Shaikin, S. Stukachev, V. Lozhkarev and A. Prokhorov, Use of KDP crystal as a Kerr nonlinear medium for compressing PW laser pulses down to 10 fs, *High Power Laser Sci. Eng.*, 2021, **9**, e54.
13 W. Ding, J. Cheng, L. Zhao, Z. Wang, H. Yang, Z. Liu, Q. Xu, J. Wang, F. Geng and M. Chen, Determination of intrinsic defects of functional KDP crystals with flawed sur-

faces and their effect on the optical properties, *Nanoscale*, 2022, **14**, 10041–10050.
14 B.-L. Wu, C.-L. Hu, F.-F. Mao, R.-L. Tang and J.-G. Mao, Highly polarizable Hg^{2+} induced a strong second harmonic generation signal and large birefringence in $LiHgPO_4$, *J. Am. Chem. Soc.*, 2019, **141**, 10188–10192.
15 S. Zhao, P. Gong, S. Luo, L. Bai, Z. Lin, Y. Tang, Y. Zhou, M. Hong and J. Luo, Tailored synthesis of a nonlinear optical phosphate with a short absorption edge, *Angew. Chem., Int. Ed.*, 2015, **54**, 4217–4221.
16 L. Wang, H. Wang, D. Zhang, D. Gao, J. Bi, L. Huang and G. Zou, Centrosymmetric $RbSnF_2NO_3$ vs. noncentrosymmetric $Rb_2SbF_3(NO_3)_2$, *Inorg. Chem. Front.*, 2021, **8**, 3317–3324.
17 T. Zheng, Q. Wang, J. Ren, L. Cao, L. Huang, D. Gao, J. Bi and G. Zou, Halogen regulation triggers structural transformation from centrosymmetric to noncentrosymmetric switches in tin phosphate halides Sn_2PO_4X (X = F, Cl), *Inorg. Chem. Front.*, 2022, **9**, 4705–4713.
18 M. Ji, C. Hu, Z. Fang, Y. Chen and J. Mao, Tin(II)-induced large birefringence enhancement in metal phosphates, *Inorg. Chem.*, 2021, **60**, 15744–15750.
19 J.-H. Wu, C.-L. Hu, T.-K. Jiang, J.-G. Mao and F. Kong, Highly birefringent d^0 transition metal fluoroantimonite in the mid infrared band: Order–disorder regulation by cationic size, *J. Am. Chem. Soc.*, 2023, **145**, 24416–24424.
20 L. Liu, Y. Li, H. Wei, M. Dong, J. Wang, A. M. Z. Slawin, J. Li, J. Dong and R. E. Morris, Ionothermal synthesis of zirconium phosphates and their catalytic behavior in the selective oxidation of cyclohexane, *Angew. Chem., Int. Ed.*, 2009, **48**, 2206–2209.
21 C. Delmas, F. Cherkaoui, A. Nadiri and P. Hagenmuller, A nasicon-type phase as intercalation electrode: $NaTi_2(PO_4)_3$, *Mater. Res. Bull.*, 1987, **22**, 631–639.
22 G. M. Sheldrick, SHELXT – Integrated space-group and crystal-structure determination, *Acta Crystallogr., Sect. A: Found. Adv.*, 2015, **71**, 3–8.
23 G. M. Sheldrick, Crystal structure refinement with SHELXL, *Acta Crystallogr., Sect. C: Struct. Chem.*, 2015, **71**, 3–8.
24 A. L. J. Spek, Single-crystal structure validation with the program PLATON, *J. Appl. Crystallogr.*, 2003, **36**, 7–13.
25 V. V. Chernaya, A. S. Mitiaev, P. S. Chizhov, E. V. Dikarev, R. V. Shpanchenko, E. V. Antipov, M. V. Korolenko and P. B. Fabritchnyi, Synthesis and investigation of tin(II) pyrophosphate $Sn_2P_2O_7$, *Chem. Mater.*, 2005, **17**, 284–290.
26 R. P. Bontchev and R. C. Moore, A series of open-framework tin(II) phosphates: $A[Sn_4(PO_4)_3]$(A = Na, K, NH_4), *Solid State Sci.*, 2004, **6**, 867–873.
27 M.-R. Li, W. Liu, M.-H. Ge, H.-H. Chen, X.-X. Yang and J.-T. Zhao, $NH_4[BPO_4F]$: A novel open-framework ammonium fluorinated borophosphate with a zeolite-like structure related to gismondine topology, *Chem. Commun.*, 2004, 1272–1273.
28 A. C. Keates, J. A. Armstrong and M. T. Weller, Iron fluorophosphates, *Dalton Trans.*, 2013, **42**, 10715–10724.
29 M. Weil, Monofluorophosphates—New examples and a survey of the PO_3F^{2-} anion, *Chemistry*, 2021, **3**, 45–73.
30 S. Boudin and K.-H. Lii, Ammonium iron(II,III) phosphate: Hydrothermal synthesis and characterization of $NH_4Fe_2(PO_4)_2$, *Inorg. Chem.*, 1998, **37**, 799–803.
31 J.-L. Song, T.-S. Guo, Z.-Y. Shi, Y.-Z. Wang, J.-Q. Cui, J.-H. Zhang and C. Zhang, Syntheses, crystal structures and luminescent properties of two new heterometallic phosphates: $Sn_2Ge(PO_4)_2(OH)_2$ and $Sn_2Mn(PO_4)_2$, *ChemistrySelect*, 2018, **3**, 1019–1023.
32 K.-Z. Du, X.-H. Qi, M.-L. Feng, J.-R. Li, X.-Z. Wang, C.-F. Du, G.-D. Zou, M. Wang and X.-Y. Huang, Synthesis, structure, band gap, and near-infrared photosensitivity of a new chalcogenide crystal, $(NH_4)_4Ag_{12}Sn_7Se_{22}$, *Inorg. Chem.*, 2016, **55**, 5110–5112.
33 X.-B. Li, C.-L. Hu, F. Kong and J.-G. Mao, Structure and optical property evolution in $PbM(PO_4)_X$ (M = Zn, Sn; X = halogen): SHG effect and birefringence, *Inorg. Chem. Front.*, 2023, **10**, 2268–2275.
34 Z. Fang, C.-L. Hu, W.-T. Chen and J.-G. Mao, $Na_3AEZn_2B_3O_9$ (AE = Mg, Ca): Two new short-wave ultraviolet beryllium-free $Sr_2Be_2B_2O_7$-type zincoborates designed by chemical cosubstitution, *Inorg. Chem. Front.*, 2022, **9**, 5188–5194.
35 J. Zhao and R. K. Li, $Ba_2(BO_3)_{1-x}(CO_3)_xCl_{1+x}$: A mixed borate and carbonate chloride crystallized from high-temperature solution, *Inorg. Chem.*, 2012, **51**, 4568–4571.
36 M. Xia and R. K. Li, Growth, structure and optical properties of nonlinear optical crystal $BaZnBO_3F$, *J. Solid State Chem.*, 2016, **233**, 58–61.
37 J. P. Perdew, K. Burke and M. Ernzerhof, Generalized gradient approximation made simple, *Phys. Rev. Lett.*, 1996, **77**, 3865–3868.
38 S. Lin, Z. Sun, B. Wu and C. Chen, The nonlinear optical characteristics of a LiB_3O_5 crystal, *J. Appl. Phys.*, 1990, **67**, 634–638.
39 J. Li, Z. Ma, C. He, Q. Li and K. Wu, An effective strategy to achieve deeper coherent light for LiB_3O_5, *J. Mater. Chem. C*, 2016, **4**, 1926–1934.
40 H. Huang, J. Yao, Z. Lin, X. Wang, R. He, W. Yao, N. Zhai and C. Chen, $NaSr_3Be_3B_3O_9F_4$: A promising deep-ultraviolet nonlinear optical material resulting from the cooperative alignment of the $[Be_3B_3O_{12}F]^{10-}$ anionic group, *Angew. Chem., Int. Ed.*, 2011, **50**, 9141–9144.
41 Z. Fang, Z.-y. Hou, F. Yang, L.-j. Liu, X.-y. Wang, Z.-y. Xu and C.-t. Chen, High-efficiency UV generation at 266 nm in a new nonlinear optical crystal $NaSr_3Be_3B_3O_9F_4$, *Opt. Express*, 2017, **25**, 26500–26507.
42 N. Ye, W. Zeng, B. Wu and C. Chen, Two new nonlinear optical crystals: $BaAl_2B_2O_7$ and $K_2Al_2B_2O_7$, electro-optic and second harmonic generation materials, devices, and applications II, SPIE, 1998, vol. 3556, pp. 21–23.

